More Effective Membrane Chromatography

Yong-Ming Wei
Chemical Engineering Research Center, East China University of Science and Technology, Shanghai 200237, China

Yanxiang Li and Chuanfang Yang
Institute of Process Engineering, Chinese Academy of Sciences, Beijing 100190, China

E. L. Cussler
Dept. of Chemical Engineering and Materials Science, University of Minnesota, Minneapolis, MN 55455

DOI 10.1002/aic.14884
Published online June 8, 2015 in Wiley Online Library (wileyonlinelibrary.com)

Adsorption in membranes with polydispersed pores gives a dispersed breakthrough curve even when mass transfer is so fast that it reaches saturation. Such a breakthrough is due to unequal flows in unequally sized pores. A theory of polydispersed pores can predict the breakthrough curves for the removal of lead ions from model solutions if the pore-size distribution is known. Such predictions are in better agreement for lead adsorption than predictions based on mass transfer. The results suggest ways in which more effective membrane chromatography can be achieved. © 2015 American Institute of Chemical Engineers *AIChE J*, 61: 3871–3878, 2015
Keywords: adsorption/liquid, membrane separations, mass transfer, chromatography

Introduction

Membrane chromatography uses a membrane as a packed bed to adsorb a solute of interest.[1–3] Because the membrane is thin, the pressure drop across the membrane is modest even when the membrane's pores are small, so that mass transfer is potentially very fast. This can potentially produce an efficient and selective separation, signaled by a sharp breakthrough curve.[4–7] In practice, such curves are usually dispersed, so membrane chromatography has not fulfilled its promise.[8–11]

Dispersed breakthrough curves are common, and result from a variety of sources. They can occur because of axial diffusion. In practice, significant axial diffusion is rare, compromising only a few cases of very low flow in high pressure liquid chromatography (HPLC). Dispersed breakthrough curves may result from Taylor–Aris dispersion, caused by coupling between axial convection and radial diffusion. This dispersion, important in analytical chromatography, means that slow diffusion causes large dispersion and fast diffusion results in small dispersion. This counterintuitive effect is the reason why the quality of separation in a chromatographic analysis is limited. Fronts can only achieve a limited sharpness.

Under industrial conditions, however, neither axial diffusion nor Taylor–Aris dispersion is especially large. A more common cause of dispersion and hence of diffuse breakthrough curves is a slow rate of mass transfer. Such a slow rate is commonly summarized by a mass-transfer coefficient k and a surface area per volume a. The mass-transfer coefficient may depend on diffusion to the pore surface and diffusion within the pores. The area per volume may vary both with the particle's external surface area and with the internal area of any pores. Both of these quantities tend to be larger as the particle size becomes smaller. This is why for analytical HPLC, the bed packing is not the characteristic 100–300 μm used in industrial scale adsorption, but is on the order of 5 μm.[12] The smaller particle size could effect much sharper breakthrough curves. However, the smaller particles cause high pressure drops which are impractical at industrial scales.

As a result, many investigations have explored "membrane chromatography," using a membrane as an adsorption bed.[13–17] The adsorbing membrane is millimeters thick, much thicker than a membrane for reverse osmosis or ultrafiltration. The pore sizes are the same as those in HPLC, about 5 μm. Such small pore sizes in a thin membrane result in rapid mass transfer but small pressure drop. Unfortunately, membrane chromatography has often been less successful in practice than expected from improved mass transfer. While the reasons for these disappointments are complex, one factor is that the breakthrough curves are not sharp. As a result, the method is used for high value added products like proteins and pharmaceuticals, but not for large-scale pollutants like heavy metal ions.

We suspect that the disappointing performance of membrane chromatography often results from the polydispersity of the pores running through the membrane. Such polydispersity produces large effects because larger pores will allow much more flow than smaller ones. As a result, the breakthrough curve will not be the desired step function, but will be dispersed. This means that only a small fraction of the bed's

Correspondence concerning this article should be addressed to E. L. Cussler at cussler@umn.edu.

possible adsorption sites will be used. It means that the bed will not be effective at all throughputs.

Below, we develop a theory for the dispersion caused by polydisperse pores. The theory assumes that mass transfer is so fast that it reaches equilibrium and that all dispersion is the result of the polydispersity. We then show that this theory explains lead removal from model solutions better than existing adsorption theories based on mass transfer. The theory also may explain some of the results for proteins and other higher value added species. We conclude by discussing how we could make beds with the equivalent of monodisperse pores.

Theory

To estimate the concentration exiting from the bed, we assume that the channels through the bed can be modeled by cylindrical pores. Such a model is approximate, but is a common starting point for many analyses of adsorption.[18] We then explore two limits. First, we review earlier theories for monodisperse pores whose performance is compromised by slow mass transfer. Second, we assume polydisperse pores in which mass transfer is so fast that each channel is saturated whenever solute is present.

Adsorption compromised by mass transfer

This standard model assumes that adsorption in a packed bed has three zones.[19,20] The first zone occurs only during the short time necessary to saturate adsorbent near the entrance of the bed, a time which we will neglect here. The second zone is a saturated region growing at a velocity v_{sat} less than actual fluid velocity v

$$v = K v_{sat} \tag{1}$$

where K is the equilibrium constant for the solute adsorption. The third "adsorption" zone is where irreversible adsorption is occurring which for a favorable isotherm has a near constant shape. The length l_A of this adsorption zone, $l_A = ka(z - v_{sat}t)$, is surprisingly independent of time, at least for a favorable isotherm. The concentration profile within this zone is

$$\frac{c}{c_0} = e^{-\frac{ka(z - v_{sat}t)}{v}} = e^{-N} \tag{2}$$

where k is a mass-transfer coefficient, a is the adsorbent area per adsorbent volume, and N is the number of transfer units. We can estimate the mass-transfer coefficient k from a correlation based on data for laminar flow in right circular cylinders[19]

$$\frac{kd}{D} = 0.8\left(\frac{dv}{\upsilon}\right)^{0.47}\left(\frac{\upsilon}{D}\right)^{1/3} \tag{3}$$

where d is the pore diameter, D is the diffusion coefficient, v is the fluid velocity, and υ is the kinematic viscosity. We will use this correlation in the predictions later in this article.

Those working in membrane chromatography expect that the membrane will have many pores of very small diameter, which have very large values of ka. They expect that the membrane pores will be short, and hence effect fast flow at modest pressure drop. Those working on membrane chromatography hope for short adsorption zones and breakthrough curves which are almost step functions.

Adsorption compromised by polydispersity

As an alternative model, we assume that the cylindrical pores are not all of equal radius, but instead have radii described by a pore-size distribution $g(R)$

$$g(R) = \frac{g(\varepsilon)}{\langle R \rangle} \tag{4}$$

where $\langle R \rangle$ is the average radius, and ε is the ratio of a radius to the average radius. The dimensionless radius ε can only be positive, so the actual radius R is given by

$$R = \langle R \rangle \varepsilon \tag{5}$$

and the differential of this radius, dR, is given by

$$dR = \langle R \rangle d\varepsilon \tag{6}$$

This radial distribution function is normalized, that is

$$\int_0^\infty g(R)dR = 1 \tag{7}$$

We can use this distribution function to calculate average properties of the membrane. For example, the average radius is

$$\int_0^\infty R g(R)dR = \int_0^\infty \langle R \rangle \varepsilon g(\varepsilon)d\varepsilon = \langle R \rangle \tag{8}$$

and the average flow $\langle Q \rangle$ is given by

$$\langle Q \rangle = \int_0^\infty \pi R^2 v g(R)dR \tag{9}$$

where v is the velocity in a pore of radius R. Because the flow is always laminar, it is described by the Hagen–Poiseuille equation

$$v = \frac{\Delta p R^2}{8\mu l} \tag{10}$$

We can use these results to find the properties of our membrane.

We now assume that mass transfer is so rapid that wherever solute and adsorptive capacity coexist in a pore, adsorption will occur instantaneously, saturating the surrounding adsorbent. A pore of a critical radius R_c will saturate when the amount of solute fed to that pore equals the amount adsorbed at equilibrium

$$\pi R_c^2 vt = K(2\pi R_c l) \tag{11}$$

or

$$R_c = \frac{2Kl}{vt} \tag{12}$$

where K is the partition coefficient of solute on the surface of adsorbent relative to that in the solution. When the radius is greater than this critical value, any solution exiting the pore will have the feed concentration c_0; when it is less, the exiting concentration will be zero. Note that this critical radius varies with time: at very small times, no pores are saturated; but at large times, they all will be. We can now calculate the concentration coming out of the membrane relative to that in the feed

$$\frac{c}{c_0} = \frac{\int_{R_c}^\infty R^4 g(R)dR}{\int_0^\infty R^4 g(R)dR} \tag{13}$$

This result gives the breakthrough curve for the case where mass transfer in the membrane is fast, where Taylor–Aris dispersion is small, but where major dispersion results from pore

Table 1. Principal Experimental Data at 25°C

Items	Units	CF	P25/CF	Anatase/CF	*In Situ*/CF
Bed void fraction	–	0.51	0.59	0.66	0.50
Fiber equilibrium capacity	mg/g	2.9	6.5	3.3	11.3
Bed equilibrium capacity	10^{-6} mol/cm^3	6.86	16.21	6.65	31.52
Bed density	g/cm^3	0.490	0.517	0.418	0.578
Bed capacity[a]	10^{-6} mol/cm^3	1.51	1.93	3.06	19.8
Fiber surface area	m^2/g	0.60	4.72	4.33	6.02
TiO_2 content	wt %	0	7.9	7.0	4.8

[a]At 10% breakthrough.

polydispersity. To make this more specific, we assume a log normal distribution of pores

$$g(\varepsilon)=\frac{1}{\varepsilon\sqrt{2\pi}\sigma}e^{-\frac{(\ln\varepsilon)^2}{2\sigma^2}} \tag{14}$$

in which ε is the dimensionless radius and σ is the standard deviation of radii. This leads to the breakthrough curve

$$\frac{c}{c_0}=\frac{\int_{\varepsilon_c}^{\infty}\varepsilon^4 g(\varepsilon)d\varepsilon}{\int_0^{\infty}\varepsilon^4 g(\varepsilon)d\varepsilon} \tag{15}$$

where $\varepsilon=R/\langle R\rangle$. The concentration in this equation is often plotted not as a function of ε, but of the dimensionless time τ defined as

$$\tau\equiv\frac{t_R}{t_{\langle R\rangle}} \tag{16}$$

where $t_R(=l/v_R)$, denotes the time needed for the solution to flow through the pores with the size of R across the membrane. By combining Eq. 16 with Hagen–Poiseuille equation (10), we can get the relationship of τ with ε

$$\tau=\frac{\langle R\rangle^2}{R^2}=\frac{1}{\varepsilon^2} \tag{17}$$

We will explore the implications of these equations in greater detail in Results section below. Before going to this section, we describe how the complimentary experiments were made.

Experimental

Materials

Experiments in this work studied adsorption of lead on different titanium dioxide (TiO_2) particles immobilized on cellulose fibers. Anatase particles (10 nm) and composite particles (P25: 30 nm, 80% anatase, and 20% rutile) were obtained from Beijing Dk Nanotechnology Co. Titanium oxysulfate solution ($TiOSO_4{\cdot}H_2SO_4{\cdot}H_2O$, ~15 wt % in dilute sulfuric acid) used to make other particles was purchased from Aldrich. Cellulose fibers of nominal 30 μm diameter (Beijing Ronel Engineering Materials Co.) were washed with distilled water before use. All other chemicals were analytical grade and used as received.

Membranes

The membranes used in this work were made from TiO_2/cellulose composite fibers prepared by either electrostatic assembly or surface reaction. In a typical electrostatic assembly, 0.1 g TiO_2 nanoparticles were suspended in 200 mL distilled water to reach a concentration of 0.5 mg/mL. After the suspension was ultrasonicated for 3 h, the pH was adjusted to 4.0 using 1 M HCl so that the particles are positively charged. Cellulose fibers, which in aqueous solution are negatively charged over a wide range of pH, were dispersed in water and collected by filtration. They were then immersed in the TiO_2 suspension. After the mixture stood for 20 min, it was filtered into a cake 47 mm in diameter and about 0.5 cm thick. After rinsing with water, the cake was dried and hot pressed using a plate drier to form a membrane. The membranes made from P25 and anatase (10 nm) were denoted as P25/CF and Anatase/CF, respectively.

Membranes were also made from particles synthesized by surface reaction on fiber surfaces. In a typical synthesis, 1.0 g cellulose fibers were suspended in 150 mL deionized water containing 2 mL sulfuric acid. Under vigorous stirring, 0.7 mL $TiOSO_4{\cdot}H_2SO_4{\cdot}H_2O$ was added dropwise. The mixture was continuously stirred at 70°C for 7 h. The fibers were then filtered, rinsed, and dried. The membranes synthesized by this method were denoted as In situ/CF. For comparison, pure cellulose fibers were also filtered to make a membrane.

Membrane properties

The pore-size distribution of all the membranes is measured with capillary flow porometry. This method records the flow rate of air through the porous membrane wet with a standard liquid having a surface tension of 16 dyne/cm. This method also requires measuring dry membrane flow and the largest pore, determined by the bubble point method.

Adsorption on the fibers used to make the membranes was studied by putting 50 mL samples of 10 mg/L lead nitrate solution and 0.04 g of fibers in 100 mL capped flasks on a platform shaker run at 150 rpm/min and 25 ± 2°C. Both 0.1 M HNO_3 and 0.1 M NaOH solution were used to adjust the pH to 6.0. The adsorption capacity q_e was calculated from

$$q_e=\frac{(c_0-c_e)}{m}V \tag{18}$$

where c_0 is the initial lead concentration, c_e is the equilibrium concentration, V is the volume of solution, and m is the mass of the fibers.

Breakthrough curves were measured by packing two layers of membrane in a filter holder, giving a total bed height of 3.0 mm, an effective bed diameter of 37 mm, and an effective bed volume of 3.2 cm^3. A feed solution containing 10 mg/L Pb^{2+} was pumped through the bed at 2.9 mL/min. The effluent samples collected vs. time were analyzed by an atomic absorption spectrometer. More details specific to particular membranes are shown in Table 1. We now consider the results.

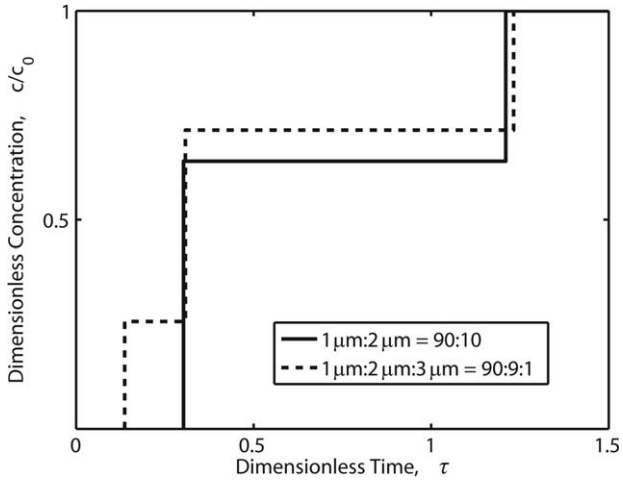

Figure 1. Predicted breakthrough curves for membranes with different sizes of pores.

As detailed in the inset, the solid line has two sizes of pores, and the dashed line was the three sizes.

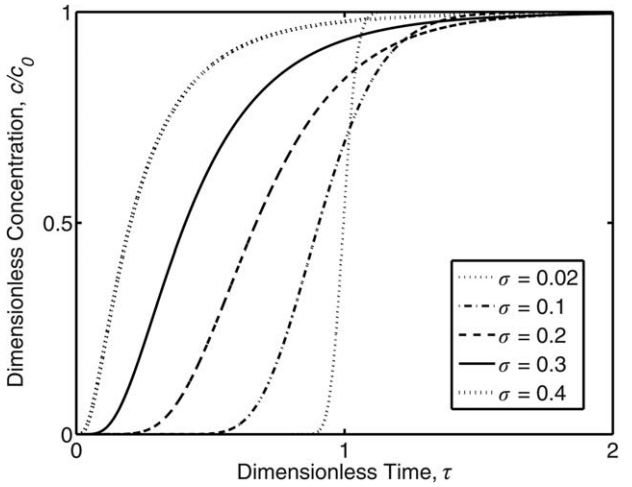

Figure 3. Predicted breakthrough curves for a log normal distribution of pore sizes.

The standard deviation of each curve is given in the inset.

Results

This article contains both theoretical and experimental results. The theoretical results center on the predictions of breakthrough curves for the cases where mass transfer is fast, but where the curves are compromised by the polydispersity. The physical experiments compare the results for lead adsorption with those estimated from models based on mass transfer and on polydispersity. These two groups of results are discussed sequentially.

The theoretical results are best understood by a series of special cases. First, we consider a membrane with pores 90% of which are 1 μm in diameter, and 10% of which are 2 μm in diameter. The pressure drop across all the pores is the same. Thus, because of the Hagen–Poiseuille law (Eq. 10), 64% of the flow goes through the 2-μm pores. The breakthrough curve, shown in Figure 1 as the solid line, has no solute coming out until the 2-μm pores saturate. Once these pores saturate but the 1-μm pores are still unsaturated, the concentration jumps to 0.64 c_0. Later, when the 1-μm pores finally saturate, the concentration jumps again, to the feed value of c_0. Thus, the membrane shows a breakthrough curve which is the superposition of two step functions. As a second special case, we consider a membrane which contains 90% 1-μm pores, 9% 2-μm pores, and 1% 3-μm pores. This shows the breakthrough given as the dashed line in Figure 1, again a superposition of step functions. As a third special case, we imagine a discrete distribution of pore sizes like those shown in the inset of Figure 2: this gives the breakthrough curve given in the main body of that figure. This is beginning to look like a real breakthrough curve.

To be more realistic, we consider log normal pore-size distributions and calculate the breakthrough curves as a function of the standard deviation σ, as shown in Figure 3. The abscissa in this figure is a dimensionless time defined as the actual time divided by the time in a pore of average diameter. Thus, a dimensionless time of greater than one refers to a pore of less than average size. As expected, these predicted curves now

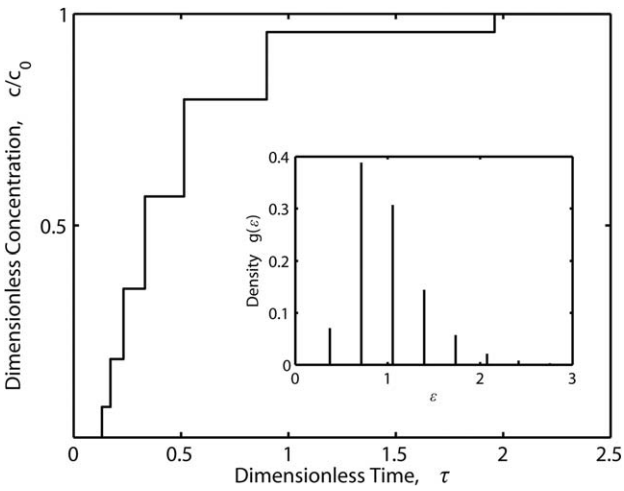

Figure 2. Predicted breakthrough curves for a membrane with a limited distribution of pore sizes.

The number and size distributions shown in the inset give a breakthrough like that observed experimentally even without mass-transfer effects.

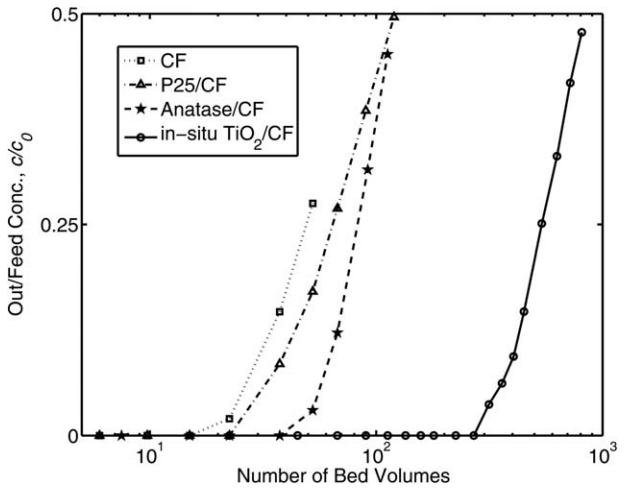

Figure 4. Experimental breakthrough curves for lead ions in titanium dioxide membranes.

Details for the membranes are given in the text.

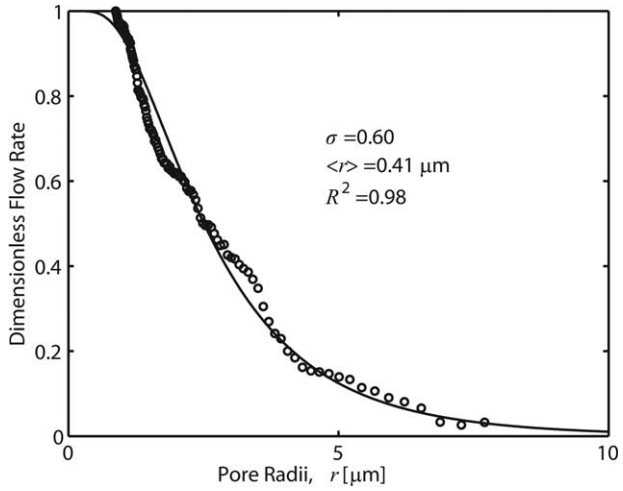

Figure 5. A typical measurement of pore-size distribution.

The solid curve, for a log normal distribution, fits the data for the in situ/CF membrane.

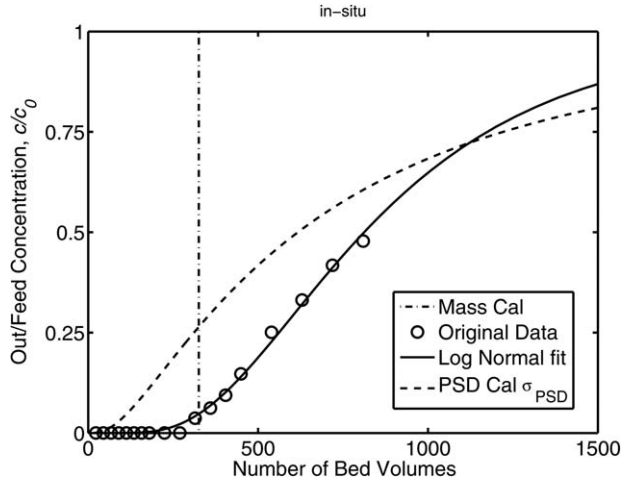

Figure 6. Experimental vs. predicted breakthrough for the in situ/CF membrane.

The solid line is the best fit using a log normal distribution of pore sizes; the dashed line is the prediction based on the measured pore-size distribution; and the uneven dashes are the prediction from mass transfer.

look like breakthrough curves typical of any adsorption experiment: they begin at zero time eluting pure solvent; and they rise with time to reach the solute concentration of the feed. Those with a sharp pore-size distribution take much longer to elute any solute, while those with a broad distribution of pores show solute exiting much earlier.

The surprise is the shape of the curves. Those with a narrow distribution of pore sizes do show a much longer time before breakthrough occurs, and those with a broad distribution do break through at much shorter times, but the slope at intermediate times does not vary that much. More detailed calculations, omitted here, show slopes at c/c_o dropping to a soft minimum for σ's between 0.1 and 0.5. We do not understand the physical reasons for this effect.

We now turn to the preliminary physical experiments made to explore the effect of polydisperse pores. To do so, we need breakthrough curves and pore-size distribution measurements. The raw data for the breakthrough curves of the four membranes are shown in Figure 4: note that the abscissa is given as the logarithm of the number of bed volumes to accommodate the wide variety of behavior observed. The measurement of pore-size distribution is exemplified by the data in Figure 5, which shows the measured distribution of the in situ/CF membrane compared by that assumed by the log normal expressions.

We can now test the mass transfer and polydispersity models against these breakthrough curves. For the mass-transfer model, we combine the data in Table 1 with Eqs. 1–3; for the polydispersity model, we use these same data and pore-size distribution measurements with Eqs. 14, 15, and 18. The results, summarized in Table 2, allow two major conclusions: first, that the mass-transfer model predicts breakthrough about 50 times later than that observed; and second, that the polydisperse model predicts breakthroughs similar to those observed, but often about two times sooner.

These conclusions are reached as follows. First, using Eq. 3, we calculate the mass-transfer coefficients expected in the membrane as shown in the first row of Table 2. Then, from Eqs. 1 and 2, we fit the experimental data in Figure 4 to find a mass-transfer rate constant ka as shown for the second row. The table shows no agreement between the values calculated from the published correlations and the values inferred from the experiments. The mass-transfer model does not work.

Next, we can compare the measured standard deviation σ of the pore-size distributions, shown in the third row of Table 2, with those inferred from Figure 4, shown in the fourth line of the table. In these inferences, we find the σ's from Eq. 15 and the log normal distribution in Eq. 14. The agreement between the σ's is reasonable, although the values from the breakthrough curves are always smaller than those from the direct polydispersity measurements. This means that the breakthrough curves measured experimentally are sharper than those expected from polydispersity. We will explore this in more detail in the discussion. Table 2 also contains σ's found for a Gaussian distribution of pore sizes, which lead to similar results to those for the log normal distribution. We have chosen the log normal distribution here feeling that it is a better approximation of our data.

We can understand these results more clearly by considering in detail the data for each of the membranes studied. The results for the most carefully studied membrane, labeled *in situ*/CF, are shown in Figure 6. The solid line in this figure is a fit of the data with a log normal pore-size distribution. The

Table 2. Sharpness Parameters from Different Models

		CF	P25/CF	Anatase/CF	In situ/CF
Mass transfer	*ka*, (correlation)	16.4	136.5	101.3	194.7
	ka, (breakthrough)	5.5	2.5	1.8	1.5
Log normal	σ, (PSD)	0.50	0.54	0.51	0.49
	σ, (breakthrough)	0.30	0.44	0.23	0.28
Gaussian	σ, (PSD)	19.1	18.8	19.9	19.1
	σ, (breakthrough)	17.9	18.9	0.82	18.7

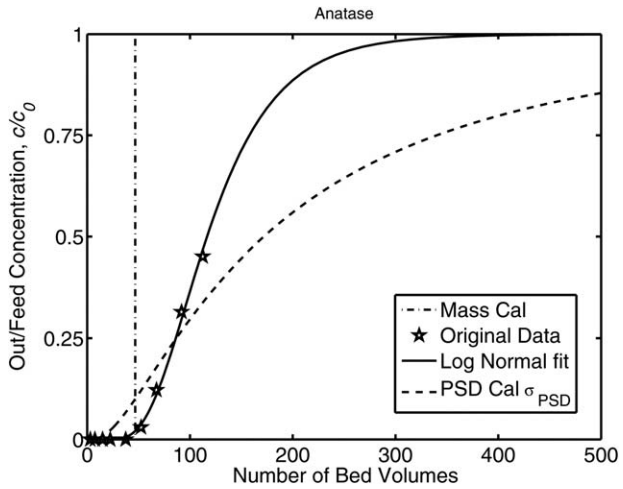

Figure 7. Experimental vs. predicted breakthrough for the anatase/CF membrane.

The lines are the analogs of those in Figure 6.

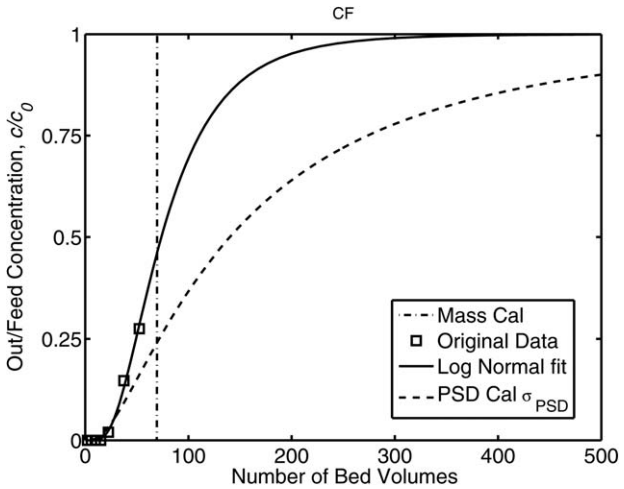

Figure 9. Experimental vs. predicted breakthrough for the CF membrane.

The lines are the analogs of those in Figure 6. This membrane contains no TiO_2.

dashed line is the prediction of the breakthrough curve, without any adjustable parameters, from Eq. 15. The third, irregularly dashed line is the prediction based on the mass-transfer correlations given in Eqs. 2 and 3. The prediction based on mass transfer, which is close to a step function, was the result sought by the original developers of membrane chromatography. This prediction does not agree with the results at all. The dashed line, that expected for polydisperse pores, shows a more gradual breakthrough than that actually observed. While this is good news, it is a surprise: we had expected that the result for polydisperse pores would be more gradual than the theoretically predicted limit, especially as polydispersity should be further compromised by noninfinite rates of mass transfer.

The data in Figure 6 are qualitatively repeated by the results for the other three membranes studied, as shown in Figures 7–9. In each of these figures, the solid curve is a best fit of the data, using a log normal pore-size distribution with the σ's collected in Table 2. While the data are fewer, they also show a breakthrough curve based on mass transfer—the irregularly dashed line—which is far sharper than the observed breakthrough curve. They show a prediction based on polydispersity—the dashed line—which is less sharp than that observed. Why this occurs is explored in the next section.

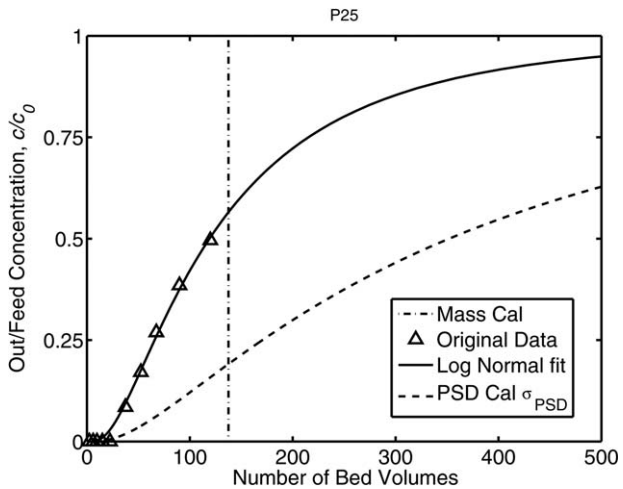

Figure 8. Experimental vs. predicted breakthrough for the P25/CF membrane.

The lines are the analogs of those in Figure 6.

Discussion

Membrane chromatography has been successful for high value products, like antibodies. It has not been as successful for dilute pollutants like heavy metal ions, primarily because breakthrough occurs well before the bed is saturated.

We believe that this inefficient bed use is not due to slow mass transfer, but to the polydispersity of the pores in the bed. In the theoretical and experimental results above, we show that the breakthrough curve expected for mass transfer is much sharper than that observed experimentally. We show that the breakthrough curve predicted from an experimentally measured distribution of pores is much closer to that observed experimentally. We should stress that these theoretical predictions are independent of whether the solute attaches on the surface, in pores or within the solid, that is, on whether adsorption or absorption is occurring. While the experimental data are preliminary, the results also show that pore-size distribution is more important than mass-transfer rate. We note that analogous effects for combined flow and mass transfer have been suggested by other authors.[21,22]

However, the results above are compromised by two unresolved questions. First, why are the experimentally observed breakthrough curves sharper than those calculated from the polydisperse pore-size distributions? Any mass transfer that slows solute uptake should make the breakthrough curves less sharp than predicted, not better. Second, if monodisperse pore-size distributions are so much better, how can we make them? After all, without this ability, knowing why we are failing is not that much help. We discuss each of these questions in turn.

While we are not sure, we believe that the better-than-expected breakthrough curves are the result of having a membrane which is a packed bed, and not one with actual cylindrical pores. In the above, we implicitly assumed that each pore goes through the membrane without any communication with any other pores. This assumption is basic to, for example, the use of the Hagen–Poiseuille equation to describe flow in each pore. But in fact, the pores are only an idealization; in fact, the

membrane is a packed bed of fibers. In such a bed, solute in a large "pore" will first saturate any adsorption sites on the fibers' walls. After this wall adsorption occurs, unadsorbed solute may both be swept further along the "pore," or may diffuse normal to the flow into other regions adjacent to the pore.

The net result of this diffusion will be to slow the progress of solute through the large pores, so that the saturation of the bed caused by the largest pores will be slowed. By reverse arguments for the smaller pores, saturation of the smaller pores will be expedited. The net effect will be a rough parallel to the Taylor–Aris dispersion which limits the separation possible in mass transfer-influenced chromatography. There, axial convection couples with radial diffusion to reduce the dispersion in the chromatographic column. Here, something somewhat similar may be happening: the broadening of the breakthrough curve caused by flow through the polydisperse pores may be reduced by diffusion normal to this flow. This "convective dispersion" would explain why the breakthrough predicted from pore polydispersity is less sharp than that observed. Verifying this speculation will require a more complete set of experiments.

We now turn to the second question important to this work: if monodisperse pores are so important, how can we make them? The results above clearly demonstrate that membrane chromatography using a membrane with monodisperse pores should give a much sharper breakthrough curve than observed with many of the membranes used for chromatography in the past. A membrane with monodisperse pores should deliver many of the advantages promised by this adsorptive separation, including a large mass-transfer coefficient, a large area per volume for adsorption, a short unused bed length, and a large throughput at modest pressure drop. However, to capture these advantages, we must have monodisperse pores or their equivalent.

There are at least four ways in which the equivalent of such pores can be realized. First, we can try to develop a block copolymer system which self assembles to give monodisperse, hexagonally close-packed cylinders. The cylinders can be aligned perpendicular to the membrane surface either by shear or by careful optimization of process conditions.[23,24] The lumen of these cylinders is then removed by etching to give the desired monodisperse pores. However, while this system could work well, the pores are typically tens of nanometers in diameter, too small for effective adsorption. These membranes have promise for selective ultrafiltration, but seem less useful here.

A second route to monodisperse pores is via lithography. In this case, a sheet of metal or polymer is lithographically masked to allow selective etching of cylindrical pores of 1–10 μm diameter, right in the range desired. Active adsorption sites are then synthesized on the surface of the pore walls. This method has real promise, although we are concerned by the high cost and the limited flexibility of some of these films. We also worry that the capacity of exchange sites per volume of membrane will be much less than that provided by conventional ion exchange. Thus, while we urge those skilled in lithography to follow this idea, we ourselves have decided to seek other routes.

The other routes center on the hope that we can achieve monodisperse pore performance with polydisperse pores if we modify the membrane geometry. These modifications presume that our real goal is to saturate the bed under conditions where mass transfer is fast. To do this, we do not need to make pores of equal diameter; we only need to make sure that the residence time through the membrane is the same in every pore. We can think of two ways to do this. In the first, we make our membrane by filtering a suspension of adsorbent fibers to make a cake. Those areas of the filter cake with faster flow will accumulate more fibers until the flow is the same through every part of the cake. We then will chemically bond the fibers to each other to make the desired membrane. Such a filter cake-membrane can be manufactured in ways similar to those currently used to make air filters.

Another method for getting monodisperse performance with polydisperse pores is to polymerize a thin ultrafiltration membrane on top of the membrane intended for chromatography. We imagine the ultrafiltration (UF) membrane will be thin, perhaps 100 nm, but have pores of tens of nanometers in diameter. The membrane for adsorption would be thicker, perhaps several millimeters across, but have pores which are tens of microns in diameter. The pressure drop through the ultrafiltration membrane will be much larger than that of the adsorbent membrane. Thus, the ultrafiltration membrane will serve as a manifold, equalizing flow through the membrane of adsorbent fibers. We look forward to exploring these ideas.

Acknowledgment

The authors are grateful to the China Scholarship Council (CSC) for awarding a scholarship under the State Scholarship Fund (No. 201306745027) and for the financial support received from the National Natural Science Foundation of China (21176067, 21276075, and 51302267).

Literature Cited

1. Tennikova TB, Bleha M, Švec F, Almazova TV, Belenkii BG. High-performance membrane chromatography of proteins, a novel method of protein separation. *J Chromatogr A*. 1991;555(1–2):97–107.
2. Roper DK, Lightfoot EN. Separation of biomolecules using adsorptive membranes. *J Chromatogr A*. 1995;702(1–2):3–26.
3. Charcosset C. Review: purification of proteins by membrane chromatography. *J Chem Technol Biotechnol*. 1998;71(2):95–110.
4. Sarin V, Singh TS, Pant KK. Thermodynamic and breakthrough column studies for the selective sorption of chromium from industrial effluent on activated eucalyptus bark. *Bioresour Technol*. 2006; 97(16):1986–1993.
5. El-Sayed MMH, Chase HA. Single and two-component cation-exchange adsorption of the two pure major whey proteins. *J Chromatogr A*. 2009;1216(50):8705–8711.
6. Santarelli X, Domergue F, Clofent-Sanchez G, Dabadie M, Grissely R, Cassagne C. Characterization and application of new macroporous membrane ion exchangers. *J Chromatogr B Biomed Sci Appl*. 1998; 706(1):13–22.
7. Bhut BV, Christensen KA, Husson SM. Membrane chromatography: protein purification from E. coli lysate using newly designed and commercial anion-exchange stationary phases. *J Chromatogr A*. 2010;1217(30):4946–4957.
8. Rao CS. Purification of large proteins using ion-exchange membranes. *Process Biochem*. 2001;37(3):247–256.
9. Avramescu M-E, Borneman Z, Wessling M. Mixed-matrix membrane adsorbers for protein separation. *J Chromatogr A*. 2003; 1006(1–2):171–183.
10. Kawai T, Saito K, Lee W. Protein binding to polymer brush, based on ion-exchange, hydrophobic, and affinity interactions. *J Chromatogr B*. 2003;790(1–2):131–142.
11. Bhut BV, Husson SM. Dramatic performance improvement of weak anion-exchange membranes for chromatographic bioseparations. *J Membr Sci*. 2009;337(1–2):215–223.
12. Lindsay S. ACOL. High performance liquid chromatography. London: Wiley, 1992.
13. Roper DK, Lightfoot EN. Estimating plate heights in stacked-membrane chromatography by flow reversal. *J Chromatogr A*. 1995; 702(1–2):69–80.

14. Santarelli X. High-performance membrane chromatography. *Biofutur*. 1997;1997(170):A6–A6.
15. Boi C, Busini V, Salvalaglio M, Cavallotti C, Sarti GC. Understanding ligand–protein interactions in affinity membrane chromatography for antibody purification. *J Chromatogr A*. 2009;1216(50):8687–8696.
16. Zeng X, Ruckenstein E. Membrane chromatography: preparation and applications to protein separation. *Biotechnol Prog*. 1999;15(6): 1003–1019.
17. Zou H, Luo Q, Zhou D. Affinity membrane chromatography for the analysis and purification of proteins. *J Biochem Biophys Methods*. 2001;49(1–3):199–240.
18. Schisla DK, Ding H, Carr PW, Cussler EL. Polydisperse tube diameters compromise multiple open tubular chromatographyw. *AIChE J*. 1993;39(6):946–953.
19. Cussler EL. *Diffusion: Mass Transfer in Fluid Systems*. Cambridge: Cambridge University Press, 2009.
20. Wankat PC. *Separation Process Engineering*. Upper Saddle River, NJ: Prentice Hall, 2011.
21. Trilisky EI, Lenhoff AM. Flow-dependent entrapment of large bioparticles in porous process media. *Biotechnol Bioeng*. 2009;104(1): 127–133.
22. Koku H, Maier RS, Schure MR, Lenhoff AM. Modeling of dispersion in a polymeric chromatographic monolith. *J Chromatogr A*. 2012;1237:55–63.
23. Phillip WA, Amendt M, O'Neill B, Chen L, Hillmyer MA, Cussler EL. Diffusion and flow across nanoporous polydicyclopentadiene-based membranes. *ACS Appl Mater Interfaces*. 2009;1(2):472–480.
24. Phillip WA, O'Neill B, Rodwogin M, Hillmyer MA, Cussler EL. Self-assembled block copolymer thin films as water filtration membranes. *ACS Appl Mater Interfaces*. 2010;2(3):847–853.

Manuscript received Dec. 17, 2014, and revision received Mar. 20, 2015.